Synthesis and Characterization of Low-Cost, N-Type Flexible Hybrid Organic/Inorganic Composite Sheets of PVDF Incorporating Ni and Cu Nanoparticles for Enhanced Electrical Conductivity and Thermoelectric Properties at Room Temperature

CHATHURANGA RATHNAYAKE[1], L.K. NARANGAMMANA[2], ROSHAN THOTAGAMUGE[3], P.G.D.C.K. KARUNARATHNA[4], P. SAMARASEKARA[5]

[1, 2, 5] *Department of Physics, Faculty of Science, University of Peradeniya, Peradeniya, Sri Lanka*

[3,4] *Department of Nano Science Technology, Faculty of Technology, Wayamba University of Sri Lanka, Kuliyapitiya, Sri Lanka*

Abstract- ***Exploring the synthesis of an n-type flexible hybrid organic/inorganic composite sheet, this study enhances PVDF with Ni and Cu nanoparticles (NP) to improve its electrical conductivity and thermoelectric properties for various room temperature applications. Ni and Cu NP, synthesized through a chemical reduction method, were smoothly incorporated into a PVDF matrix. The optimal NP to PVDF ratio was determined to be 2:3 (wt), as further addition of particles led to the formation of cracks and weakened the flexibility of the sheet. The synthesized materials' elemental composition, including Ni and Ni-Cu composites in various ratios, was analyzed using XRF, aligning closely with expected ratios and highlighting synthesis precision. FTIR spectroscopy specifies molecular structures and phases in PVDF-based nanocomposites. XRD patterns confirmed Ni and Cu NP presence and revealed trends in PVDF behavior with decreasing particle size. SEM imaging depicted well-defined particles and surface coverage in PVDF/Ni sheets, with additional Cu resulting in reduced particle density on the polymer surface, indicating compositional correlation The highest power factor, 4.964 μW m^{-1} K^{-2} and figure of merit, 0.003, were achieved at 298 K for the composite with the weight ratio of PVDF/Ni (2:3). The four-probe method demonstrated an impressive conductivity of 25.64 S cm^{-1} at 298 K. Furthermore, Seebeck coefficient showed a - 44 μV K^{-1} indicating n-type behavior, and thermal conductivity was 0.5 W m^{-1} K^{-1}, which is consistent with the low thermal conductance required for effective thermoelectric materials. Excessive addition of Cu nanoparticles to the PVDF/Ni composite disrupts optimal Ni-PVDF interaction, impeding continuous conductive pathways and diminishing electrical conductivity and thermoelectric properties, highlighting the need for precise composite formulation. Tensile strength and elastic modulus measurements were conducted, highlighting the flexibility of the developed thermoelectric material. This study lays the foundation for the successful creation of a low-cost, n-type flexible thermoelectric material using Ni nanoparticles and PVDF.***

Indexed Terms- ***PVDF, Ni nanoparticles, Flexible, n-type, Thermoelectric, Power factor***

I. INTRODUCTION

The integration of conducting polymers, particularly organic polymers, in the realm of thermoelectric materials has marked a significant advancement, offering prospects for flexible applications in wearable electronics. However, the prevalent challenge of intrinsic p-type conductivity in most conducting polymers, such as polyaniline, polythiophene, and polypyrrole, has created a noteworthy imbalance in the availability of n-type and p-type materials [1–4]. This asymmetry poses a critical limitation in the development of balanced and efficient thermoelectric systems, crucial for optimizing device performance. While strategies involving the chemical modification of p-type polymers and the creation of hybrid materials have been explored to address this issue, the scarcity of effective n-type conducting polymers remains a persistent challenge. In light of the

expanding field of wearable thermoelectric devices, overcoming this limitation is essential for unlocking the full potential of flexible thermoelectric materials and realizing advancements in energy harvesting from body heat. Understanding the distinction between p-type and n-type conductivity is essential for tailoring thermoelectric materials to specific applications. In the case of wearable thermoelectric devices, where flexibility, efficiency, and adaptability are crucial, achieving a balance between n-type and p-type materials becomes imperative [5]. Overcoming the limitation in the availability of effective n-type conducting polymers is pivotal for realizing the full potential of flexible thermoelectric materials in wearable electronics and energy harvesting from body heat.

The pressing concerns of environmental pollution and energy shortages have fueled the pursuit of green energy conversion approaches, where thermoelectric materials have emerged as promising candidates for sustainable and eco-friendly energy solutions. These materials, capable of direct and reciprocal conversion of thermal and electrical energy, play a pivotal role in the development of energy-saving technologies. Their small size, high reliability, pollution-free characteristics, and versatility across a wide temperature range make them integral to the advancement of sustainable energy applications.

Traditionally, inorganic semiconductors like BiSb, Bi_2Te_3, and PbTe have been the focal points in thermoelectric materials due to their high thermoelectric figure of merit (ZT). However, their intrinsic brittleness and high cost hinder large-scale energy conversion processes. On the other hand, organic polymer thermoelectric materials, such as PEDOT, PANI, PTh, and PPy, offer advantages like low cost, high flexibility, and ease of processing. Nevertheless, their thermoelectric conversion efficiency tends to be relatively low [6–9]

The marriage of high-performance inorganic materials with easily synthesized, flexible polymers has emerged as a compelling approach to maximize the benefits of both material classes. Composite materials resulting from this integration exhibit appealing thermoelectrical properties, attracting substantial research attention. Noteworthy examples include the addition of tin selenide (SnSe) nanosheets to PEDOT: PSS, resulting in a composite with enhanced thermoelectric properties and a figure of merit reaching up to 0.32 [10–12]. Similarly, the combination of n-type and p-type Bi_2Te_3 powders into PEDOT: PSS has yielded composites with high Seebeck coefficient and power factor.

While previous research has predominantly focused on combining polymers with inorganic semiconductor materials, the exploration of polymer and metal thermoelectric composites has been relatively limited. Nickel, abundant in the Earth's crust and possessing favorable properties such as ductility, magnetism, and corrosion resistance, presents a compelling opportunity for such composites. PVDF, with its diverse crystal structures, chemical resistance, weather resistance, dielectric properties, and thermoelectric potential, serves as an effective partner in these composites [13].

Chen et al.'s work on PVDF/Ni nanowire composites achieved an ultrahigh power factor value of 220 $\mu Wm^{-1} K^{-2}$, showcasing the potential of combining nickel and PVDF for highly efficient thermoelectric materials [7]. The study discussed the preparation method for high aspect ratio Ni nanowires and their embedding in PVDF to form n-type composite thermoelectric materials. Investigation into the effects of different nickel nanowire compositions on the thermoelectric properties revealed a remarkable 4000-fold increase in conductivity when the nickel nanowire content reached 75 wt%. Furthermore, the study delved into the mechanical properties of the composite, emphasizing the flexibility of the materials [7].

In conclusion, while advancements in thermoelectric materials have predominantly focused on inorganic semiconductors and polymer-inorganic composites, the exploration of polymer and metal thermoelectric composites, exemplified by PVDF/Ni nanowire composites, represents a promising and less-explored avenue. The combination of nickel's favorable properties with PVDF's versatility opens new possibilities for highly efficient and flexible thermoelectric materials, catering to diverse requirements in energy harvesting and wearable electronics.

Polyethylenedioxythiophene has been extensively employed to fabricate flexible thermoelectric materials owing to its electrical conductivity [14–16]. In addition, Carbon based materials find potential applications in flexible thermoelectric generators due to their remarkable electrical conductivity, thermal stability, and excellent mechanical strength [17–19]. Power output as high as 3.8 W has been attained for a compound of reduced graphene oxide, Ce, Fe, Co, Yb, and Sb [20,21]. Thermovoltage of 600 mV has been generated by non-oxidized graphene flakes with lanthanum strontium titanium oxide [22]. Among inorganic thermoelectric materials, compounds with Bi, Sb, Te, and Se have reported a figure of merit value of 1.2 [23].

In this study, we aim to create an n-type nanocomposite by adding Ni nanoparticles to the PVDF matrix and investigate the effect of adding different amounts of Cu to the PVDF/Ni matrix on its thermoelectric and mechanical properties.

II. MATERIALS AND EXPERIMENTAL

A. Materials

All the chemicals used were analytical grade chemicals, such as: Hydrazine hydrate solution ($N_2H_4.H_2O$), Nickel chloride hexahydrate ($NiCl_2.6H_2O$), Copper chloride dihydrate ($CuCl_2.2H_2O$), Sodium hydroxide (NaOH), Polyvinylidene fluoride (PVDF), and N,N-dimethylsulfoxide (DMSO).

B. Synthesis of nickel nanoparticles

Ni nanoparticles were synthesized by a common liquid-phase chemical reduction method as follows. First, 0.5 g of $NiCl_2.6H_2O$ was dissolved in a beaker containing 40 ml of deionized water and 20 ml of ethanol. Then 1.5 g of NaOH solid particles were added and stirred vigorously until completely dissolved. Next, 20 ml of hydrazine hydrate solution was added dropwise into the above solution at a flow rate of 1 ml/min. While adding the reducing agent, the solution turned royal blue and was heated at 200 ℃ for 1 h. The prepared Ni nanoparticles were then separated by magnets and washed several times using deionized water and ethanol, respectively. Finally, it was placed in a vacuum drying oven and dried at room temperature for 1 h [7,24].

C. Synthesis of Ni-Cu (4:1) weight ratio nanocomposite

Ni-Cu (4:1) nanocomposite was synthesized by a common liquid-phase chemical reduction method. First, 0.4 g $NiCl_2.6H_2O$ and 0.1 g of $CuCl_2.2H_2O$ were dissolved in a beaker containing 30 ml of deionized water and 20 ml of ethanol. Then 1.5 g of NaOH solid particles were added and stirred vigorously until completely dissolved. Next, 20 ml of hydrazine hydrate solution was added dropwise into the above solution at a flow rate of 1 ml/min. While adding the reducing agent (N_2H_4), the solution turned brown. After that, the solution was sonicated for 1 h and the solution turned black. Then, the solution was heated at 200 °C for 1 h. The prepared Ni-Cu nanocomposites were then separated by magnets and washed several times using deionized water and ethanol, respectively. Finally, it is placed in a vacuum drying oven and dried at room temperature for 1 h [7, 24].

D. Synthesis of Ni-Cu (3:2) weight ratio nanocomposite

Ni-Cu (3:2) nanocomposite was synthesized by a common liquid-phase chemical reduction method. First, 0.3 g of $NiCl_2.6H_2O$ and 0.2 g of $CuCl_2.2H_2O$ were dissolved in a beaker containing 30 ml of deionized water and 20 ml of ethanol. Then 1.5 g of NaOH solid particles were added and stirred vigorously until completely dissolved. Next, 20 ml of hydrazine hydrate solution was added dropwise into the above solution at a flow rate of 1 ml/min. While adding the reducing agent (N_2H_4), the solution turned brown. After that, the solution was sonicated for 1 h and the solution turned black. Then, the solution was heated at 200 °C for 1 h. The prepared Ni-Cu nanocomposites were then separated by magnets and washed several times using deionized water and ethanol, respectively. Finally, it was placed in a vacuum drying oven and dried at room temperature for 1 h [24].

E. PVDF, PVDF/Ni, PVDF/Ni/Cu, composite film preparation process

A flexible PVDF sheet was fabricated as follows. First, 0.2 g of polyvinylidene fluoride (PVDF) powder and 3 ml of DMSO were mixed in a beaker and magnetically stirred at 70 ℃ for half an hour until completely dissolved. Then, the mixed solution was

placed in a vacuum drying oven and dried at 40 °C for 12 h.

PVDF/Ni, PVDF/Ni/Cu, composite sheets were synthesized as follows. 0.2 g of PVDF powder and 3 ml of DMSO were mixed in a beaker and magnetically stirred at 70 ℃ for half an hour until completely dissolved. Further, different content of Ni based nanocomposite powder was added and ultrasonically shaken at 50 ℃ for 1 h to uniformly disperse the nanoparticles in the mixed solution. Then, the mixed solution was placed in a vacuum drying oven and dried at 40 ℃ for 12 h to prepare a PVDF sheet.

F. Characterizations

The determination of particle size in the synthesized Ni particles constitutes a pivotal aspect of this investigation, accomplished through the utilization of Dynamic light scattering (DLS) particle size analysis. The resulting samples were subjected to X-ray Fluorescence (XRF) analysis to confirm their elemental composition. The samples were analyzed using a "Jasco FT/IR-6000" FTIR spectrometer to confirm the successful synthesis of Polyvinylidene fluoride (PVDF) and explore the influence of Ni and Cu additives on the structural changes and molecular interactions of PVDF. The structural properties of samples were determined by a Rigaku Ultima IV X-ray diffractometer with Cu-Kα (λ = 1.5406 Å) radiation. The surface morphology of films was explored by a Zeiss EVO LS15 Scanning Electron Microscope (SEM). The sheet resistance of films was measured using a Jandel model (RM3000+). The electrical conductivity of samples was found by means of a Keithley 6400 sourcemeter AUTOLAB.

To measure the Seebeck coefficient and ascertain the temperature difference across the sample, rectangular shape samples with a width of 1 cm and a length of 2 cm were employed. Subsequently, a heater was employed, and a small porcelain plate was positioned atop the heater, serving as a base for a vertically placed copper rod secured by a lab stand clamp. Another copper rod was situated 2 cm apart from the first one at the same height, fastened by an additional clamp. The sample was then positioned atop these two copper rods. Thermocouples and voltage probes from the Keithley multimeter were intricately connected to the copper rods to facilitate the measurement of temperature and voltage differences. To precisely measure the voltage, the Keithley multimeter played a pivotal role. The heater, responsible for generating the temperature difference, was heated by supplying current. Subsequently, the resultant temperature and voltage differences were symmetrically measured for each sample. This meticulous experimental setup not only allowed for the accurate determination of the Seebeck coefficient but also contributed valuable data to the comprehensive thermoelectric characterization of the synthesized nanocomposite sheets.

The thermal conductivity of sheets was measured using the absolute steady-state axial flow method. To determine the thermal conductivities of the sheets, a similar approach was adopted. A porcelain plate was positioned atop the heater, serving as a base for a vertically placed copper rod. Another copper rod was situated at the same height, but 2 cm away from the first one. The sample was then horizontally placed on these two copper rods. Subsequently, two digital thermometers equipped with thermocouples were intricately connected to the copper rods to measure temperatures at the two ends of the sample. A constant power supply was provided to the heater, and once a steady state was achieved, temperatures were measured. During this stable state, the current passing through the heater and the voltage were measured using two multimeters.

The mechanical testing machine, also known as the tensile testing machine, is used to obtain the tensile properties of materials, such as the ultimate tensile strength, yield strength, elongation, and elastic modulus. The mechanical testing machine is designed so that one end of the sample is pulled up while the other end is fixed by attaching it to a load cell to monitor the applied load. In order to pull the sample without torsion, a ball screw is used, and it converts the stepping motor rotation into linear rotation. A ball screw positioned in line with the specimen provides the tensile force. A linear motion guide is adopted for precise alignment of the specimen without any distortion during gripping and tensile loading. A computer system is connected to the mechanical testing machine so that the application software gives a graph of applied load vs. time.

III. RESULTS AND DISCUSSION

A. XRF results analysis

Table I shows the comprehensive analysis of the elemental composition of the synthesized materials, including Ni nanoparticles and Ni-Cu composites in 4:1 and 3:2 ratios, using X-ray Fluorescence (XRF) to precisely determine the constituent elements. For the Ni nanoparticle sample, the XRF results indicated a dominant presence of Ni accounting for 99.83%, along with trace amounts of Yttrium 0.09%, iron 0.06%, and manganese 0.03%, as shown in Table I.

Table I: XRF analysis results for the synthesized nanoparticles.

Sample	Percentage (wt %)				
	Ni	Cu	Y	Fe	Mn
Ni	99.83	-	0.09	0.06	0.03
Ni-Cu (4:1)	79.62	20.13	0.10	0.08	0.07
Ni-Cu (3:2)	61.61	38.19	0.12	0.06	0.02

In the 4:1 ratio Ni-Cu nanocomposite, the elemental analysis revealed a composition of 79.62% Ni and 20.13% Cu. Similarly, for the 3:2 ratio Ni-Cu nanocomposite, the XRF data showcased a composition of 61.61% Ni and 38.19% Cu. The accuracy of the results is evident in the elemental composition obtained through XRF analysis, showcasing a close alignment with the expected ratios. The method's success in yielding Ni and Cu nanoparticles in different ratios, as verified by XRF, underscores the precision of the synthesis approach. This accuracy can be attributed to the careful control of reaction parameters, including the choice of reducing agent and pH adjustment, contributing to the successful conversion of metal chlorides into nanoparticles.

B. Fourier transform infrared spectroscopy (FTIR) analysis

Fig. 1 shows the characterization of distinct vibrational bands in synthesized PVDF based nanocomposites using FTIR spectroscopy. The analysis revealed several key bands associated with specific crystalline phases of PVDF. Bands at approximately 763 cm^{-1} and 1228 cm^{-1} were identified as characteristic of the α-phase. Concurrently, bands at 868 cm^{-1}, 1165 cm^{-1} and 1400 cm^{-1} were attributed to the β-phase. These findings provide a detailed insight into the vibrational signatures associated with different phases of PVDF, aiding in the comprehensive characterization of the synthesized samples.

In the FTIR spectrum of PVDF, the observed peaks at specific wavenumbers provide valuable information about the molecular structure and different phases of the polymer [25–30]. The PVDF crystallinity is indicated by several peaks. The first peak, 763 cm^{-1}, is associated with in-plane bending/rocking in the alpha phase, indicating crystallinity. The second peak, 831 cm^{-1}, is associated with the CH_2 out of plane wagging mode. The third peak, 868 cm^{-1}, is related to the rocking vibration of CH_2 groups and the asymmetric stretching vibrations of CF_2 groups in the beta phase. The fourth peak, 1070 cm^{-1}, is attributed to the stretching vibration of CF groups. The fifth peak, 1165 cm^{-1}, is related to the stretching vibration of CF_2 groups in the beta phase, indicating variations in molecular conformations and crystalline arrangements. The sixth peak, 1228 cm^{-1}, is indicative of the alpha phase, corresponding to the asymmetric stretching vibration of CF_2 groups. The last peak, 1400 cm^{-1} is associated with the CH_2 scissoring mode in the beta phase.

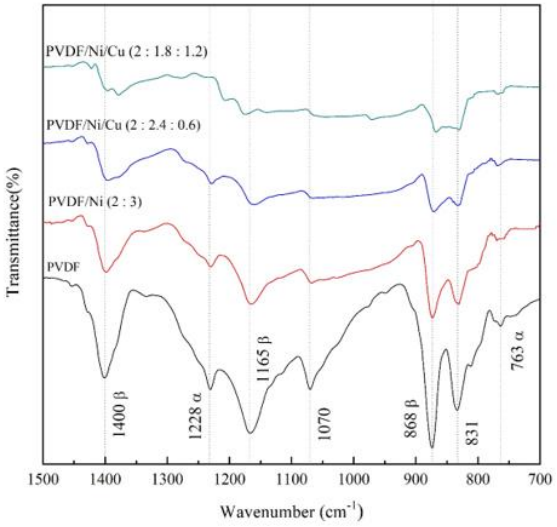

Fig. 1: FTIR transmission spectrum of the synthesized composite sheets.

In the FTIR analysis of PVDF and its nanocomposite variants, intriguing trends were observed in the intensity of the characteristic peaks. When incorporating PVDF with Ni in a 2:3 weight ratio, a noticeable decrease in peak intensity was observed. Further addition of Cu to form PVDF/Ni/Cu nanocomposites, specifically in ratios of (2:2.4:0.6) and (2:1.8:1.2), resulted in a continuous reduction in peak intensity. This trend was more pronounced as the Cu content increased, suggesting a correlation between Cu concentration and the observed changes in the FTIR spectra of PVDF.

This observed decrease in peak intensity, especially with higher Cu ratio, could be attributed to the smaller particle sizes of these nanoparticles. The competition for space within the polymer matrix, particularly when adding nanoparticles with reduced sizes, appears to influence the FTIR spectra. These findings emphasize the importance of nanoparticle size considerations in nanocomposite formulations and their subsequent impact on the molecular structure and interactions within the composite material.

Additionally, comparing these findings with previous studies [7], which used Ni nanowires instead of nanoparticles, reveals interesting parallels and distinctions. While both studies observed a decrease in peak intensity with the incorporation of nickel-based materials into the PVDF matrix, this research extends this understanding by exploring the effects of Cu nanoparticles alongside Ni nanoparticles. This broader investigation provides valuable insights into how different nanoparticle compositions influence the molecular interactions and structural properties of PVDF-based nanocomposites.

C. XRD analysis of the samples

Fig. 2 shows the expected peaks unveiled by XRD patterns, as anticipated [7,24,31–34]. These peaks confirm that the synthesized nanoparticles were exactly Ni and Cu. And the PVDF peaks are identified as the β – phase of PVDF. However, a fascinating revelation emerged as to the behavior of PVDF amidst the introduction of various nanoparticles. Upon introducing Nickel, the PVDF peak took a subtle step back, revealing a minor decrease. Yet, when Copper joined the mix, the PVDF peak underwent a more noticeable descent. This intriguing phenomenon aligns seamlessly with the trends in the FTIR graph. It's as if PVDF becomes more spacious when the particle sizes decrease. The distinctive responses of Cu suggest a more profound interaction with PVDF compared to the relatively milder interaction with Nickel. The XRD patterns serve as a visual representation of these dynamics, reinforcing the idea that the decrease in particle size leads to a more pronounced influence on the PVDF matrix.

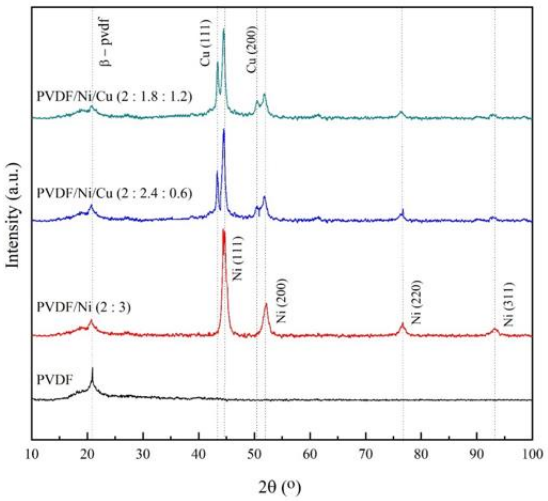

Fig. 2: XRD spectrum of the synthesized composite sheets.

In comparing the XRD findings with previous research [7,24], noticeable similarities and differences become apparent, providing insights into how nanoparticle morphology and composition influence the structural properties of PVDF-based nanocomposites. The XRD patterns of PVDF/Ni NW composites in one of the studies [7] show a dominant presence of Nickel nanowires, overshadowing the weak PVDF diffraction peaks. In contrast, the XRD analysis with Ni nanoparticles demonstrates that the PVDF peaks are clearly identified, suggesting a more homogeneous dispersion of nanoparticles within the matrix. Additionally, another study [24] highlights challenges associated with Ni and Cu peaks overlapping in PVDF/Cu-Ni bulk material, attributed to the cold pressing process used to create cubes. In our study, focused on flexible materials without such processing, the distinct peaks of Ni and Cu are clearly identified without overlapping, indicating a more favorable dispersion and interaction within the PVDF matrix.

The Debye Scherrer equation was precisely applied to determine the crystallite sizes of nickel and copper in the PVDF matrix [35,36]. For nickel nanoparticles, the average size was 89.28 nm, with various crystallite orientations including (111), (200), (220), and (311), revealing sizes ranging from 79.97 nm to 99.66 nm. Similarly, for copper nanoparticles, the average size was 42.62 nm, with crystallite orientations including (111) and (200), unveiling sizes ranging from 46.51 nm to 38.73 nm. These sizes provide crucial insights into the structural properties of the composite, elucidating the configuration of atoms within the nanoparticles and their impact on material characteristics.

The smaller crystallite sizes of the copper nanoparticles allowed them to occupy more spaces within the PVDF matrix, influencing the material's overall structure and properties. This phenomenon was observed in the XRD analysis, where the PVDF peak decreased in intensity with the addition of copper, as depicted in Fig. 2. Additionally, the variations in crystallite sizes between nickel and copper nanoparticles contribute to the unique characteristics of the composite material. Nickel's larger crystallite sizes indicate a denser arrangement within the PVDF matrix, potentially enhancing its conductivity. On the other hand, the smaller crystallite sizes of copper suggest a more dispersed distribution, which could enhance the flexibility of the composite. Understanding these nuances in crystallite sizes and their impact on the composite's structure is vital for tailoring its properties to specific application requirements.

The precision of our analysis, supported by the Debye Scherrer equation, underscores the reliability of our results and emphasizes the intricate relationship between synthesis processes, nanoparticle dispersion, and crystalline morphology in the PVDF matrix. This comprehensive approach, rooted in fundamental crystallographic principles, enhances our understanding of the synthesis and structural dynamics of nanocomposites, facilitating the intelligent optimization of material properties for diverse applications.

These observations suggest a more complex picture of the interactions between nanoparticles and the PVDF matrix. This deep XRD analysis vividly captures the success of nanoparticle synthesis and their interactions within the PVDF material.

D. SEM images of the samples

Fig. 3 shows the high-magnification SEM images of the sample sheets. The Ni particles, as shown in Fig. 3 (b), exhibited a spherical shape, with the PVDF/Ni sheet displaying particularly clear and well-defined particles compared to the other samples, with a determined diameter of 368 nm. This clarity indicated that the larger particle size of nickel allowed for more effective coverage of the PVDF matrix surface. Moreover, the high-magnification images depicted most of the nickel particles in the PVDF/Ni sheet being stacked one by one, forming a strong bond with the PVDF matrix. In contrast, the other sheets displayed fewer particles on the surface. Fig. 3 (c) revealed a small nanorod. By considering the addition of more Cu to the matrix, it resulted in fewer particles on the surface, likely due to the smaller particle sizes of these materials. In addition to the observed particle characteristics, noteworthy features were identified during the SEM analysis. In Fig. 3 (c), certain anomalies were observed, including the presence of cracks. These cracks could be attributed to various factors, such as changes in the composition of the sample or variations in the synthesis process. The cracks may have resulted from stresses induced during the preparation or drying stages. While the cracks in Fig. 3 (c) were noticeable, they were not prevalent in the other samples.

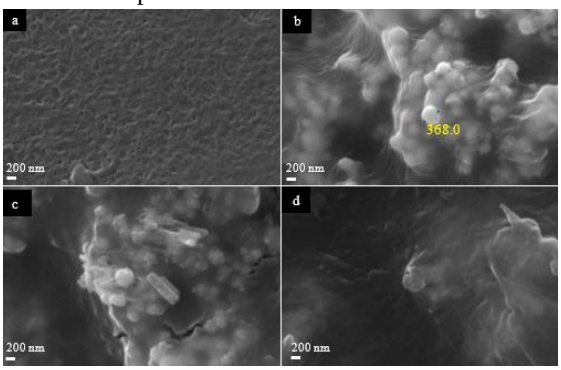

Fig. 3: SEM images of the synthesized composite sheets at high magnification (50 K) (a) PVDF, (b) PVDF/Ni (2:3), (c) PVDF/Ni/Cu (2:2.4:0.6), (d) PVDF/Ni/Cu (2:1.8:1.2).

Fig. 4 shows the low-magnification SEM images of the sample sheets. Examining the low magnification images uncovered voids on the surface of the PVDF matrix, as evident in Fig. 4 (a). The introduction of nickel to the PVDF filled these voids, covering the entire surface with particles. However, Fig. 4 (c) and (d) show persistent voids, suggesting that additional Cu led to fewer particles on the polymer surface. The observations from both high and low magnification images provide insights into the distribution, bonding, and coverage of particles on the PVDF matrix in response to varying compositions.

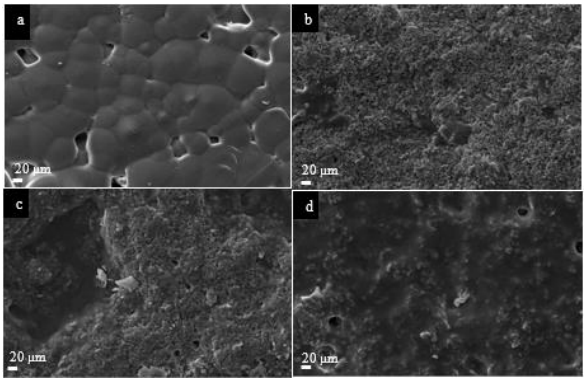

Fig. 4: SEM images of the synthesized composite sheets at low magnification (1 K) (a) PVDF, (b) PVDF/Ni (2:3), (c) PVDF/Ni/Cu (2:2.4:0.6), (d) PVDF/Ni/Cu (2:1.8:1.2).

In addition to the detailed SEM analysis presented, it's noteworthy to consider the insights gained from a comparative perspective with a previous study [7]. In their investigation, Ni nanowires were utilized instead of nanoparticles, resulting in distinct structural characteristics and behavior within the PVDF matrix. The SEM images from the previous study revealed that higher Ni NW content in the PVDF composite led to increased brittleness, with significant cracking observed at elevated Ni NW concentrations. However, this study with Ni nanoparticles reveals a nuanced understanding of particle-matrix interactions, showcasing particularly clear and well-defined particles with a larger diameter, enabling more effective coverage of the PVDF matrix surface. While both studies observed stacking behavior, indicative of good dispersibility, these findings underscore the advantages of employing Ni nanoparticles, with their larger size and uniform dispersion contributing to enhanced bonding and coverage on the polymer surface. These comparative insights highlight the superior performance and potential of Ni nanoparticles in PVDF-based nanocomposites, offering valuable guidance for the design and optimization of advanced materials [7].

E. Electrical conductivity

Table II shows the analysis results obtained using the four-probe method in the subsequent phase of the study. The measured sheet resistance, along with the current values, facilitated the calculation of resistivity and conductivity for each sample. The obtained data reveal distinct electrical behaviors across the various compositions.

Sheet resistance of thin sheet is given by,

$$R = \frac{\pi}{ln\,(2)}\left(\frac{V}{I}\right)$$

Bulk resistivity of thin sheet is given by,

$$\rho = R \times t$$

Where V, I, and t are the voltage, current, and thickness, respectively.

For the PVDF sheet, a minimal current of 10 nA and a voltage of 118.91 mV resulted in a high sheet resistance of 5.39 × 107 Ω/sq. The resistivity and conductivity values were calculated as 10.78 × 105 Ω cm and 0.93 × 10-6 S cm^{-1}, respectively. Incorporating nickel (PVDF/Ni 2:3 weight ratio) significantly altered the electrical characteristics, evident in the substantial increase in current (10 mA), reduction in sheet resistance (1.97 Ω/sq), and an increase in conductivity to 25.64 S cm^{-1} as shown in Table II. Similarly, the introduction of copper (PVDF/Ni/Cu) led to distinctive changes in the electrical properties, showcasing the tunability of the composite materials.

Notably, variations in the Cu to Ni ratios influenced the sheet resistance, resistivity, and conductivity in the PVDF/Ni/Cu samples, providing insights into the role of each component in determining the electrical performance of the composites. These findings contribute valuable information for optimizing the electrical characteristics of the synthesized materials for specific applications in electronic devices and thermoelectric applications.

Table II: Results for the bulk resistivity and bulk conductivity by the four probe method for the sheets.

Composite Sheet	I ($\times 10^{-3}$A)	V ($\times 10^{-3}$V)	Sheet resistance (Ω/sq)	Resistivity ($\times 10^{-1}$ Ω cm)	Conductivity (S cm^{-1})
PVDF/Ni (2:3)	10.00	4.34	1.97	0.39	25.64
PVDF/Ni/Cu (2:2.4:0.6)	10.00	18.03	8.17	1.63	6.13
PVDF/Ni/Cu (2:1.8:1.2)	0.10	0.45	20.40	4.10	2.44

Given the 2D nature of the materials under study, the conventional approach of utilizing the four-probe method for electrical conductivity measurement is often preferred; however, due to potential sample cracking affecting probe alignment and readings, employing a comparative analysis using the two-probe method offers valuable insights. The electrical conductivity values measured by Autolab Potentiostat were obtained through plotting I-V curves for the samples and subsequently calculating resistance and conductivity values.

The electrical conductivity of the sample is given by,

$$\sigma = \frac{l}{RA} \quad (3)$$

Where R, A and l are the resistance, cross sectional area, and length of the sample, respectively.

For the PVDF sample, no specific resistance (R) value or conductivity could be determined, highlighting the nonlinearity of the formed I-V curves for this sheet.

In contrast, the PVDF/Ni composites (2:3 wt ratio) demonstrated a resistance of 7.62 Ω and a conductivity of 23.21 S cm^{-1}, showcasing enhanced electrical properties compared to the pristine PVDF. However, when incorporating Cu into the composites, variations in resistance and conductivity were observed. The PVDF/Ni/Cu (2:2.4:0.6) composition displayed a resistance of 35.37 Ω and a conductivity of 4.99 S cm^{-1}, while the PVDF/Ni/Cu (2:1.8:1.2) composition showed a higher resistance of 196.48 Ω and a lower conductivity of 0.90 S cm^{-1}.

The comparison between the four-probe method and the Autolab Potentiostat approach reveals distinct advantages and limitations. In the four-probe method, the use of four small probes minimizes contact surface, reducing interfacial resistance and enabling precise measurements of bulk properties. Conversely, the Autolab Potentiostat method employs only two electrodes, resulting in a higher contact surface and potentially higher interfacial resistance. These differences in contact surface and resistance may contribute to variations in measured conductivity values, emphasizing the importance of understanding methodological differences when interpreting results. Considering the obtained results, discrepancies between the two methods, such as slightly lower conductivity measured by the Autolab Potentiostat method for samples, could be attributed to interfacial resistance at the electrodes due to the higher contact area. These findings underscore the importance of considering the measurement technique and electrode interactions when assessing the electrical properties of composite material sheets (2-D material).

In the previous study [7], which utilized Ni nanowires in the PVDF matrix, the electrical conductivity exhibited a significant increase with increasing nickel nanowire content. For instance, when the content of nickel nanowires increased from 60 wt% to 75 wt%, the conductivity surged from 3.62 S cm^{-1} to 252.6 S cm^{-1}. This behavior aligns with the percolation threshold theory, where the composite's conductivity sharply rises beyond a critical filler content.

In our study, however, we encountered limitations when attempting to increase the nickel nanoparticle content up to 75 wt%. It was observed that beyond a certain threshold, the formation of the 2D material film sheet was compromised, leading to cracking. Specifically, only at the 3:2 ratio (60 wt%) could a stable film sheet be formed. Consequently, at this ratio, the electrical conductivity for the nickel nanoparticle composite was measured at 25.64 S cm^{-1}, compared to 3.62 S cm^{-1} for the nickel nanowire composite in the previous study. This difference

suggests that a significant portion of the nickel nanoparticles may have accumulated on the surface of the PVDF matrix, potentially enhancing surface conductivity.

In another study [24], bulk materials were synthesized by incorporating Ni-Cu alloy into the PVDF matrix, resulting in electrical conductivity values ranging from 225.4 S cm^{-1} to 817.0 S cm^{-1} at 325 K for composites with weight ratios of 1/4, 1/6, and 1/8, respectively. This conductivity was notably higher than that observed in our study (flexible material), where nickel nanoparticles were dispersed in the PVDF matrix. One possible explanation for this disparity could be the difference in synthesis methods: the previous study involved creating an alloy prior to incorporation into the polymer matrix, while our study simply involved adding separate Ni-Cu nanoparticles. Moreover, variations in synthesis processes and resulting structures between bulk materials and flexible composites may have influenced the observed differences in electrical conductivity. Additionally, the previous study conducted measurements at elevated temperatures, while our study focused on room temperature, which could have impacted conductivity values due to changes in carrier mobility and concentration. Variability in reported conductivity values can arise from factors like measurement technique choice, instrument accuracy, sample preparation, electrode contact quality, and measurement conditions, affecting reliability and reproducibility.

F. Seebeck coefficient

The seebeck coefficient values of the synthesized composite sheets were measured at 298 K. However, due to experimental challenges and inherent errors, the Seebeck coefficient values for PVDF sample could not be precisely determined.

Seebeck coefficients were calculated for each sample at room temperature using,

$$\alpha = -\frac{\Delta V}{\Delta T} \quad (4)$$

The potential difference across the material with the temperature values at the hot and cool ends was measured.

Despite these difficulties, the measured values for the other compositions at room temperature (298 K) provide valuable insights. For the PVDF/Ni (2:3) composite, a Seebeck coefficient of - 44 µV K^{-1} was obtained, indicating its potential for thermoelectric applications. The PVDF/Ni/Cu (2:2.4:0.6) and PVDF/Ni/Cu (2:1.8:1.2) composites exhibited Seebeck coefficients of - 40 µV K^{-1} and - 38 µV K^{-1}, respectively. These values suggest that the introduction of Cu to the Ni-based composite slightly reduces the Seebeck coefficient, possibly due to altered charge carrier dynamics. The obtained negative values of the Seebeck coefficient for the synthesized composite sheets unequivocally confirm their n-type behavior. The negative Seebeck coefficients affirm the predominant flow of electrons as the charge carriers, contributing to the material's potential for efficient thermoelectric energy conversion.

Comparing our study with the findings of previous research provides valuable insights into the influence of composition and material structure on thermoelectric properties. In [7], where nickel nanowires were incorporated into the PVDF matrix, increasing the Ni nanowire content from 30 wt% to 75 wt% resulted in a decrease in the Seebeck coefficient from -32.68 µV K^{-1} to -31.01 µV K^{-1}. In contrast, our study achieved a significantly higher Seebeck coefficient of -44 µV K^{-1} at room temperature for a composition containing 60 wt% nickel nanoparticles. This substantial improvement can be attributed to several factors. Firstly, the morphology and dispersal of the nickel nanoparticles within the PVDF matrix may have facilitated more efficient charge carrier transport, leading to enhanced thermoelectric performance. Additionally, the intrinsic properties of nickel nanoparticles, such as their higher surface area and conductivity compared to nanowires, could have contributed to the observed improvement in the Seebeck coefficient.

Furthermore, comparing with [24], where Ni-Cu alloys were utilized to create bulk materials, our study offers a contrasting perspective. In [24], an increase in the Seebeck coefficient from -49.23 µV K^{-1} to -50.45 µV K^{-1} was observed when adding more Ni-Cu alloys to the PVDF matrix. This higher Seebeck coefficient in bulk materials could be attributed to several factors. Firstly, the formation of an alloy between Ni and Cu

may have resulted in enhanced electron transport properties and reduced scattering of charge carriers, leading to improved thermoelectric performance. Additionally, the bulk nature of the material provides a more continuous conductive pathway, minimizing interfacial resistance and further enhancing the Seebeck coefficient. In our study, when incorporating Ni-Cu nanoparticles into the PVDF matrix to create flexible thermoelectric materials, we observed a decrease in the Seebeck coefficient. This contrasts with the findings in [24], where the Seebeck coefficient increased when Ni-Cu alloys were added to PVDF to produce bulk materials. The disparity in results highlights the intricate interplay between composition, morphology, and processing methods in determining thermoelectric properties. One possible explanation for the decrease in Seebeck coefficient in our study could be the heterogeneous distribution of Ni-Cu nanoparticles within the flexible composite, leading to increased scattering of charge carriers and reduced overall thermoelectric performance. Conversely, the formation of a uniform alloy phase in bulk materials may facilitate more efficient charge transport, resulting in the observed increase in the Seebeck coefficient in [24]. These contrasting outcomes underscore the importance of considering material structure and processing techniques in optimizing thermoelectric materials for diverse applications.

Interestingly, the trends observed in the changes of Seebeck coefficient values with varying composition differ between [7] and [24]. In [7], the Seebeck coefficient decreased with increasing nickel nanowire content, while in [24], it increased with the addition of more Ni-Cu alloys. In our study, we achieved an intermediate Seebeck coefficient value, resembling the trend observed in [24]. This suggests that factors such as material morphology, composition, and processing techniques play critical roles in determining thermoelectric performance. By elucidating these relationships, our research contributes to advancing the understanding of thermoelectric materials and provides insights for future optimization and design strategies.

G. Thermal conductivity

Thermal conductivity values of the synthesized composite sheets were measured at 298 K. The thermal conductivity values obtained for the fabricated composite sheets were crucial parameters that influenced their performance as thermoelectric materials. Thermal conductivity was calculated for the sheets at room temperature using the absolute steady-state axial flow method.

$$K = \frac{IVL}{\Delta T} \quad (5)$$

Where I, V, L and ΔT are the current, voltage, length of the sample and temperature difference respectively. The thermal conductivity of the base material, PVDF, was measured as 0.32 W m^{-1} K^{-1}. Interestingly, the introduction of nickel (PVDF/Ni) (2:3) wt ratio shows an increase in thermal conductivity to 0.50 W m^{-1} K^{-1}, suggesting that the incorporation of nickel contributes to enhancing heat transfer properties. Further modifications in the form of PVDF/Ni/Cu composites demonstrate a controlled rise in thermal conductivity (0.52 and 0.53 W m^{-1} K^{-1} for wt ratios 2:2.4:0.6 and 2:1.8: 1.2, respectively). This indicates a fine-tuning of thermal characteristics, potentially beneficial for specific applications.

In this study, the observed trends in thermal conductivity values can be attributed to several factors. The increase in thermal conductivity upon the introduction of nickel (PVDF/Ni) suggests that nickel may possess superior thermal transport properties compared to PVDF alone. Nickel, being a highly conductive metal, could facilitate more efficient heat transfer within the composite material. The controlled rise in thermal conductivity with the addition of copper to the PVDF/Ni composites (PVDF/Ni/Cu) indicates a synergistic effect between nickel and copper, possibly enhancing thermal conductivity through improved interfacial coupling and conductivity pathways.

Comparing with previous research [24], where Ni-Cu alloys were added to the PVDF matrix to create bulk materials, the slightly lower thermal conductivity values observed in our study could be due to differences in the composite structure and processing methods. Bulk materials may have a more continuous conductive pathway, leading to enhanced thermal conductivity compared to flexible composites. Additionally, the experimental temperature differences between studies could influence thermal

conductivity measurements, as thermal conductivity often varies with temperature.

H. Power Factor and Figure of merit

Table III shows the power factor and figure of merit values of the synthesized composite sheets at 298 K. For the PVDF/Ni (2:3) composite, a notable power factor of 4.964 μW m^{-1} K^{-2} was achieved at 298 K, contributing to an impressive ZT of 29.58×10^{-4}. This suggests that the incorporation of nickel into the PVDF matrix enhances its thermoelectric properties, making it a promising material for thermoelectric applications.

Power factor (*PF*) and the figure of merit (*ZT*) are given by,

$$PF = \alpha^2\sigma \quad (6)$$

$$ZT = \frac{\alpha^2\sigma T}{K} \quad (7)$$

Table III: Power factor and figure of merit values of the sheets at 298 K.

Composite Sheet	Power Factor (μW m^{-1} K^{-2})	ZT (× 10^{-4})
PVDF	-	-
PVDF/Ni (2:3)	4.964	29.58
PVDF/Ni/Cu (2:2.4:0.6)	0.981	5.62
PVDF/Ni/Cu (2:1.8:1.2)	0.352	1.98

However, as the composition is modified to PVDF/Ni/Cu (2:2.4:0.6) and PVDF/Ni/Cu (2:1.8:1.2), the power factors decrease to 0.981 μW m^{-1} K^{-2} and 0.352 μW m^{-1} K^{-2}, respectively, as shown in Table III. Consequently, the ZT values also diminish, indicating a compromise in the thermoelectric performance. The decline in these parameters may be attributed to the introduction of copper, which has a lower Seebeck coefficient compared to nickel, impacting the overall power generation capability of the material. Unfortunately, the lack of Seebeck coefficients for PVDF hinders the calculation of power factors and ZT values for these specific sheets.

Comparing our study with previous research reveals significant differences in power factor trends, underscoring the distinctive aspects of our methodology. For example, in [7], we observed a higher power factor at a 60% nickel ratio compared to theirs. However, it's crucial to highlight that they could integrate up to 75% Ni nanowires into PVDF, whereas we utilized Ni nanoparticles. This variance in material morphology likely impacted the observed power factor values. Unlike prior studies that employed compressed nanowires in the PVDF matrix, our approach involved dispersing nanoparticles within the matrix, potentially leading to lower power factors due to variations in charge carrier transport mechanisms.

Similarly, in [24], higher power factors were attained by crafting bulk materials through increased Ni-Cu alloy incorporation into the PVDF matrix. Conversely, our emphasis on flexible materials might have contributed to the observed decrease in power factor. This discrepancy underscores the trade-offs between material flexibility and thermoelectric performance, with bulk materials exhibiting higher power factors, while our flexible approach opens avenues for applications necessitating flexibility and conformability.

Furthermore, studies [37] and [38] achieved higher power factors by introducing Cu_2Se and Ag_2Se nanowires into the PVDF matrix compared to our study. Notably, their use of nanowires differed from our nanoparticle approach, likely influencing power factor values. Additionally, while prior studies compressed materials, our uncompressed nanoparticle approach may have impacted the power factor. These distinctions highlight the importance of considering material morphology and processing techniques in optimizing thermoelectric properties. Despite our study's lower power factors, our approach offers benefits in flexibility and dispersion control, catering to tailored applications requiring flexible thermoelectric materials.

I. Tensile strength and elastic modulus

The mechanical properties of the prepared sheets play an integral role in their application as an efficient, flexible thermoelectric material. Here, the tensile strength and elastic modulus of the prepared sheets were evaluated through a tensile test using a mechanical testing machine A computer system is connected to the mechanical testing machine so that the application software gives a graph of applied load

vs. time. Using those data, the strain and stress values were calculated to plot the graph.

Stress vs. strain graphs were plotted for the samples.

$$\frac{F}{A} = Y\left(\frac{\varepsilon}{l}\right) \quad (8)$$

Where F, A, Y, ε, and l are the force exerted by the sample, effective cross-sectional area, elastic modulus, extension, and length of the sample, respectively.

Table IV shows that in the case of pure PVDF, the elastic modulus was measured as 47.95 MPa, indicating a robust and resilient nature, coupled with a tensile strength of 4.38 MPa. Upon introducing nickel into the composite (PVDF/Ni 2:3), the elastic modulus experiences a decrease to 30.81 MPa, and the tensile strength decreases to 2.13 MPa. These changes suggest a slight compromise in the mechanical properties due to the incorporation of nickel, potentially attributed to the alteration of the composite's structural characteristics.

Table IV: Tensile strength and elastic modulus values for the sheets.

Composite Sheet	Elastic modulus (MPa)	Tensile strength (MPa)
PVDF	47.95	4.38
PVDF/Ni (2:3)	30.81	2.13
PVDF/Ni/Cu (2:2.4:0.6)	32.14	2.54
PVDF/Ni/Cu (2:1.8:1.2)	33.86	2.46

Similarly, for the PVDF/Ni/Cu composite sheets, with compositions (2:2.4:0.6) and (2:1.8:1.2), the elastic modulus varies from 32.14 MPa to 33.86 MPa, and the tensile strength varies from 2.54 MPa to 2.46 MPa, as shown in Table IV. These values indicate that the introduction of copper into the composite has a moderate impact on the mechanical properties, with the material maintaining a balance between flexibility and strength.

In this study, we observed a notable pattern in the tensile strength and elastic modulus of the synthesized composite sheets. For instance, in comparison to previous work such as [7], which exhibited a similar pattern of tensile strength to ours but with higher values, we attribute this difference to factors such as the compressing process and the utilization of nanowires instead of nanoparticles. The compressing process in previous studies might have facilitated better alignment and packing of the nanowires within the matrix, leading to enhanced mechanical properties. Additionally, the intrinsic mechanical properties of nanowires, such as their high aspect ratio and strong interfacial interactions, could contribute to the observed higher tensile strength. Conversely, our approach with nanoparticles dispersed within the matrix may have led to less efficient load transfer and weaker interfacial bonding, resulting in lower tensile strength and elastic modulus values. Nonetheless, our decision to explore and analyze mechanical properties alongside thermoelectric performance adds depth to our understanding of these composite materials and paves the way for their application in various fields where mechanical integrity is paramount.

Table V: Thermoelectric properties and tensile strength of PVDF matrix composites reported in recent years.

Matrix	Filler	Electrical conductivity (S/cm)	Seebeck coefficient (μV K^{-1})	PF (μW m^{-1} K^{-2})	Tensile strength (MPa)	Ref
PVDF	Ni NW	252.6	-31.01	24.3	25	[7]
PVDF	Cu-Ni alloy	760.5	-49.90	189.7	-	[24]
PVDF	Cu2Se NW	5578	14.16	111.8	-	[37]
PVDF	Cu-Bi2Se3	146	-84	103.2	-	[39]

PVDF	Te nanorod	5.5	288	45.8	-	[40]
PVDF	Ni NP	25.6	-44	5.0	4.38	This work

CONCLUSION

This study delved into synthesizing and characterizing hybrid materials by incorporating nickel nanoparticles into polyvinylidene fluoride (PVDF) matrices, aiming to develop an n-type flexible thermoelectric material. By applying nanocomposite engineering principles, we optimized composition to tailor the electrical and thermoelectric properties of these hybrids. Through systematic experimentation, the PVDF/Ni (2:3) weight ratio emerged as optimal, yielding uniform composites with superior thermoelectric characteristics. Despite PVDF's insulating nature, the inclusion of Ni nanoparticles significantly boosted electrical conductivity to 25.64 S cm^{-1}, showcasing the transformative effect of nanocomposite engineering. Moreover, remarkable thermoelectric performance metrics were observed, including n-type behavior with a Seebeck coefficient of -44 µV K^{-1} at 298 K, a power factor of 4.964 µW m^{-1} K^{-2}, and a figure of merit of 0.003 at 298 K, marking a significant advancement in thermoelectric materials. Furthermore, comparing our results with those of previous studies [7] and [24], our approach offers distinct advantages. While [7] demonstrated higher electrical conductivity in PVDF/Ni NW composites (252.6 S cm^{-1}), our method provides a simpler and more economical route, with a significantly lower cost associated with producing and incorporating nanoparticles compared to nanowires. Additionally, [24] utilized Ni-Cu alloy additives to create bulk PVDF composites, which observed an increase in thermoelectric properties. In contrast, our study showcases a different trend by prioritizing flexibility over bulkiness, achieving commendable thermoelectric performance while maintaining favorable mechanical properties. However, augmenting PVDF/Ni matrices with additional elements like Cu led to diminished electrical and thermoelectric properties compared to the PVDF/Ni composite. SEM imaging revealed insights into these interactions, highlighting variations in particle distribution and bonding within the composite. XRD and FTIR patterns further elucidated how the addition of Cu affected the composite's structure. Nonetheless, despite these challenges, the PVDF/Ni (2:3) weight ratio composite exhibited favorable flexibility and retained promising thermoelectric properties, showcasing its resilience and potential for real-world applications. Additionally, our materials exhibit promising thermoelectric properties at room temperature, making them suitable for wearable thermoelectric devices. Looking ahead, further research should explore alternative configurations and processing methods to maximize thermoelectric performance and broaden the understanding of these materials across different operating conditions.

REFERENCES

[1] A. Bhattacharya and A. De (1996). Conducting composites of polypyrrole and polyaniline: A review. Progress in Solid State Chemistry, 24.

[2] M.I. Khan, et al. (2021). Conductive polymers and their nanocomposites as adsorbents in environmental applications. Polymers, 13, article ID 3810.

[3] V. Cavalheiro Maeda, et al. (2023). Electrical and mechanical properties of self-supported hydroxypropyl methylcellulose-polyaniline conducting films. RSC Advances, 13, 7913–7920.

[4] S. Liu, H. Li, P. Li, Y. Liu and C. He (2021). Recent advances in polyaniline-based thermoelectric composites. CCS Chemistry, 3, 2547–2560.

[5] S. Zhu, et al. (2022). Review on wearable thermoelectric generators: From devices to applications. Energies, 15, article ID 3375.

[6] T. Wu, et al. (2022). Dual post-treatments boost thermoelectric performance of PEDOT:PSS films and their devices. Macromolecular Materials and Engineering, 307.

[7] S. Hu, et al. (2020). Flexible and high performance of n-type thermoelectric PVDF composite film induced by nickel nanowires. Materials and Design, 188.

[8] S. Sun, M. Li, X.L. Shi and Z.G. Chen (2023). Advances in ionic thermoelectrics: From

materials to devices. Advanced Energy Materials, 13.

[9] R. Rai, J.A. Roether and A.R. Boccaccini (2022). Polyaniline based polymers in tissue engineering applications: A review. Progress in Biomedical Engineering, 4.

[10] E. Jin Bae, Y. Hun Kang, K.S. Jang and S. Yun Cho (2016). Enhancement of thermoelectric properties of PEDOT:PSS and tellurium-PEDOT:PSS hybrid composites by simple chemical treatment. Scientific Reports, 6.

[11] R. Brooke, et al. (2023). Nanocellulose and PEDOT:PSS composites and their applications. Polymer Reviews, 63, 437–477.

[12] S. Yang, P. Qiu, L. Chen and X. Shi (2021). Recent developments in flexible thermoelectric devices. Small Science, 1.

[13] L. Xie, G. Wang, C. Jiang, F. Yu and X. Zhao (2021). Properties and applications of flexible poly(vinylidene fluoride)-based piezoelectric materials. Crystals, 11.

[14] O. Bubnova, et al. (2011). Optimization of the thermoelectric figure of merit in the conducting polymer poly(3,4-ethylenedioxythiophene). Nature Materials, 10, 429–433.

[15] Y. Du, J. Xu, B. Paul and P. Eklund (2018). Flexible thermoelectric materials and devices. Applied Materials Today, 12, 366–388.

[16] M. Sattar and W.H. Yeo (2022). Recent advances in materials for wearable thermoelectric generators and biosensing devices. Materials, 15.

[17] X. Wang, H. Wang and B. Liu (2018). Carbon nanotube-based organic thermoelectric materials for energy harvesting. Polymers, 10.

[18] J.S. Yun, S. Choi and S.H. Im (2021). Advances in carbon-based thermoelectric materials for high-performance, flexible thermoelectric devices. Carbon Energy, 3, 667–708.

[19] J. Choi, et al. (2019). High-performance, wearable thermoelectric generator based on highly-aligned carbon nanotube sheet. ACS Applied Energy Materials, *3*(1), 1199-1206.

[20] P.A. Zong, et al. (2017). Skutterudite with graphene-modified grain-boundary complexion enhances zT enabling high-efficiency thermoelectric device. Energy & Environmental Science, 10, 183–191.

[21] R. Mulla, A.O. White, C.W. Dunnill and A.R. Barron (2023). The role of graphene in new thermoelectric materials. Energy Advances, *2*(5), 606-614.

[22] J. Tse, et al. (2021). Unraveling the impact of graphene addition to thermoelectric SrTiO3 and La-doped SrTiO3 materials: A density functional theory study. ACS Applied Materials & Interfaces, 13, 41303–41314.

[23] M.M. Mallick, et al. (2021). Realizing high thermoelectric performance of Bi-Sb-Te-based printed films through grain interface modification by an in situ-grown β-Cu2-δSe phase. ACS Applied Materials & Interfaces, 13, 61386–61395.

[24] I. Paulraj, V. Lourdhusamy and C.J. Liu (2022). Organic/inorganic n-type PVDF/Cu0.6Ni0.4 hybrid composites for thermoelectric application: A thermoelectric generator made of 8 pairs of p-leg ZnSb/Sb and n-leg β-PVDF/Cu0.6Ni0.4. Chemical Engineering Journal, 446.

[25] T.S. Roopa, H.N. Murthy, D.V.N. Harish, A. Jain and G. Angadi (2021). Properties of PVDF films stretched in machine direction. Polymers and Polymer Composites, 29, 198–206.

[26] S. Lanceros-Méndez, J.F. Mano, A.M. Costa and V.H. Schmidt (2001). FTIR and DSC studies of mechanically deformed β-PVDF films. Journal of Macromolecular Science, Part B: Physics, 40, 517–527.

[27] A. Salimi and A.A. Yousefi (2003). FTIR studies of β-phase crystal formation in stretched PVDF films. Polymer Testing, 22, 699–704.

[28] K.A.R. Medeiros, et al. (2018). Evaluation of the electromechanical behavior of polyvinylidene fluoride used as a component of risers in the offshore oil industry. Oil and Gas Science and Technology, 73.

[29] X. Cai, T. Lei, D. Sun and L. Lin (2017). A critical analysis of the α, β and γ phases in poly(vinylidene fluoride) using FTIR. RSC Advances, 7, 15382–15389.

[30] B. Mohammadi, A. A. Yousefi and S. M. Bellah (2007). Effect of tensile strain rate and elongation on crystalline structure and piezoelectric properties of PVDF thin films. Polymer testing, *26*(1), 42-50.

[31] F. Bonet, et al. (2003). Synthesis and characterization of bimetallic Ni-Cu particles. Journal of Solid State Chemistry, 172, 111–115.

[32] T. He, et al. (2022). Poly(vinylidene fluoride) (PVDF) membrane fabrication with an ionic liquid via non-solvent thermally induced phase separation (N-TIPS). Applied Water Science, 12.

[33] A.D. Prasetya, M. Rifai, Mujamilah and H. Miyamoto (2020). X-ray diffraction (XRD) profile analysis of pure ECAP-annealing Nickel samples. Journal of Physics: Conference Series, 1436, 012113.

[34] N.H. Lam, et al. (2022). Powder X-ray diffraction analysis of Cu/Cu2O nanocomposites synthesized by colloidal solution method. Korean Journal of Chemical Engineering, 39, 2505–2512.

[35] M. I. Zakirov, M. P. Semen'Ko, & O. A. Korotchenkov (2018). A simple sonochemical synthesis of nanosized ZnO from zinc acetate and sodium hydroxide. Journal of Nano-and Electronic Physics, 10(5).

[36] S. Mustapha, M. M. Ndamitso, A. S. Abdulkareem, J. O. Tijani, D. T. Shuaib, A. K. Mohammed and A. Sumaila (2019). Comparative study of crystallite size using Williamson-Hall and Debye-Scherrer plots for ZnO nanoparticles. Advances in Natural Sciences: Nanoscience and Nanotechnology, 10(4), 045013.

[37] S. Pammi, V. Jella, J.-S. Choi and S.-G. Yoon (2017). Enhanced thermoelectric properties of flexible $Cu_{2-x}Se$ ($x \geq 0.25$) NW/polyvinylidene fluoride composite films fabricated via simple mechanical pressing. Journal of Materials Chemistry C, 5(3), 763–769.

[38] H. Zhou, Z. Zhang, C. Sun, H. Deng, & Q. Fu (2020). Biomimetic approach to facilitate the high filler content in free-standing and flexible thermoelectric polymer composite films based on PVDF and Ag_2Se nanowires. ACS Applied Materials & Interfaces, 12(46), 51506-51516.

[39] C. Dun, C. A. Hewitt, H. Huang, J. Xu, C. Zhou, W. Huang, Y. Cui, W. Zhou, Q. Jiang and D. L. Carroll (2015). Flexible n-type thermoelectric films based on Cu-doped Bi_2Se_3 nanoplate and polyvinylidene fluoride composite with decoupled Seebeck coefficient and electrical conductivity. Nano Energy, 18, 306–314.

[40] C. Dun, C. A. Hewitt, H. Huang, D. S. Montgomery, J. Xu and D. L. Carroll (2015). Flexible thermoelectric fabrics based on self-assembled tellurium nanorods with a large power factor. Physical Chemistry Chemical Physics, 17(14), 8591–8595.